Construction of Multi-scale Common Brain Networks Based on DICCCOL

Bao Ge[1], Lei Guo[2], Dajiang Zhu[3], Tuo Zhang[2,3], Xintao Hu[2], Junwei Han[2], and Tianming Liu[3]

[1] College of Physics & Information Technology, Shaanxi Normal University, Xi'an, China
[2] School of Automation, Northwestern Polytechnical University, Xi'an, China
[3] Cortical Architecture Imaging and Discovery Lab, Department of Computer Science, University of Georgia, Athens, GA, USA

Abstract. Modeling the human brain as a network has been widely considered as a powerful approach to investigating the brain's structural and functional systems. However, many previous approaches focused on a single scale of brain network and the multi-scale nature of brain networks has been rarely explored yet. This paper put forward a novel framework to construct multi-scale common networks of brains via multi-scale spectral clustering of fiber connections among DICCCOLs. Specifically, the recently developed and publicly released DICCCOLs provide the nodal structural and functional correspondence across individuals, and thus the employed multi-scale spectral clustering algorithm divided the DICCCOL landmarks and their connections into sub-networks with correspondences on multiple scales. Experimental results showed the promise of the constructed multi-scale networks in applications of structural and functional connectivity mapping. As an application example, these multi-scale networks are used to guide the identification of multi-scale common fiber bundles across individuals and to facilitate the bundle's functional role analysis, which could enable other tract-based and network-based analyses in the future.

Keywords: DTI, multi-scale common brain networks, fiber clustering, DICCCOL.

1 Introduction

Whole-brain anatomical and functional connectivity in living humans can be modeled as networks via diffusion MRI and fMRI data. Typically, network nodes are associated with distinct grey-matter regions of interest (ROIs), and edges are defined as fiber pathways or functional correlations between cortical ROIs. Then, graph theory based network analysis can be applied to reveal the brain's network properties in a variety of applications [1, 14, 15]. However, despite the growing importance of studying networks in the human brain mapping community, construction of brain network still faces two general challenges. The first is the lack of accurate nodal correspondence across individuals and populations. In general, there has been no gold standard for regional parcellation in the brain, which makes the definition of network nodes uncertain. For instance, network nodes can be defined by employing either template-based warping or based on certain parcellation criteria [5]. In fact, the

J.C. Gee et al. (Eds.): IPMI 2013, LNCS 7917, pp. 692–704, 2013.

template registration method has difficulty in dealing with the remarkable variation of cortical folding patterns in individual brains. Without the nodal correspondences between brain networks, many meaningful and comparative statistical measurements of network properties cannot be accurately performed. Second, many previous studies defined network nodes at a single spatial scale without consideration of the intrinsic multi-scale nature of brain networks. Essentially, recent research has demonstrated that the structural and functional connectivity occurs at multiple spatial levels [10, 14-15], and thus how to find the optimal scales and determine the number/size of nodes is vitally important to construct brain networks.

Recently, we developed and publicly released the DICCCOL (Dense Individualized and Common Connectivity-based Cortical Landmarks) system [1]. These identified and validated 358 group-wise consistent DICCCOL landmarks possess intrinsically-established structural and functional correspondences across individuals [1]. Importantly, they have been well reproduced in over 240 individual brains [1]. Thus, these 358 landmarks offer a universal and individuated brain reference system. In particular, these 358 landmarks can be accurately predicted in each individual brain with DTI data [1]. Thus, these DICCCOL landmarks can be used as the corresponding nodes for brain network construction to deal with the abovementioned first challenge. The DICCCOL software toolkit has been released on NITRC [11], and Figure 1(a) shows an example of these 358 DICCCOL landmarks.

In this paper, by treating the DICCCOL landmarks as the basic network nodes, we constructed the corresponding brain networks in multiple scales by an effective multi-scale spectral clustering algorithm [2]. Specifically, the DTI-derived fiber connection strength between DICCCOL landmarks is used as the feature of clustering based on the principle of functional segregation and integration [12]. Importantly, the correspondences are kept among the network nodes in multiple scales by group-wise averaging of the connectivity matrices across different subjects. Since the basic correspondences have been established by DICCCOLs, the optimal scales and the sizes/numbers of node are determined by the multi-scale spectral clustering. We have applied this novel methodology on a DTI dataset, and promising and meaningful results have been achieved. In particular, as an application example, the multi-scale networks are used to guide the multi-scale fiber clustering and reasonable results were obtained. Finally, we analyzed the functional roles for each sub-network and fiber bundle via meta-analysis [3] of the BrainMap fMRI activation database [7]. In general, the major methodological contributions of this paper are the introduction, evaluation and application of a general framework for multi-scale common network construction based on structural connectivity patterns and for multi-scale common fiber clustering, which can potentially enable other structural and functional modeling and mapping of brain networks in the future.

2 Methods

2.1 Overview

The flowchart of our multi-scale brain network construction includes the following steps. First, we pre-processed the raw DTI data, and tracked the whole-brain fibers via the streamline method. Then, we predicted the 358 corresponding and consistent

DICCCOL landmarks for each brain via the methods in [1]. By treating these DICCCOL landmarks as the primitive nodes, on which we computed the connectivity matrix based on the streamline fiber connections, then an effective multi-scale spectral algorithm was applied to determine the multiple scales and to cluster nodes into clusters with the optimal size/number.

2.2 Data Acquisition and Preprocessing

Nine healthy young adults recruited at The University of Georgia (UGA) under UGA IRB approval were scanned in a GE 3T Signa MRI system (GE Healthcare, Milwaukee, WI) using an 8-channel head coil at the UGA Bioimaging Research Center (BIRC), Athens, GA. Diffusion tensor imaging (DTI) data were acquired using the isotropic spatial resolution 2mm×2mm×2mm; parameters were TR 15.5s and TE min-full, b-value = 1000 with 30 DWI gradient directions and 3 B0 volumes acquired. Pre-processing of the DTI data included brain skull removal, motion correction, and eddy current correction. After the pre-processing, the whole-brain streamline tractography was performed using the MEDINRIA toolkit (FA threshold: 0.2; minimum fiber length: 20). Then, we predicted the DICCCOL landmarks using the open-source toolkit in [11].

2.3 The Dissimilarity Measure of Landmarks

The theory of functional segregation and integration considers that human brains might have been competitively selected to maximize the cost efficiency of parallel information processing in large-scale networks [12]. That is, brain evolution tends to increase its efficiency (favoring the selection of a few long-range axonal fiber connections mediating efficient information transfer between spatially distributed regions) while decrease the cost (favoring a high density of short-range local connections), like an economical small-world network. According to this principle, we can divide the brain network by its local connection or its DTI-derived streamline fiber connections. However, since current DTI and tractography techniques cannot track the local connection in gray matter, we can only seek alternative methods. In our previous paper [13], the local affinity was measured by using geodesic distance to construct multi-scale brain networks, in that those cortical regions with small distances are likely to connect each other by short-range intra-column connections. In this paper, instead, we adopt the DTI-derived fiber connection (long-range connection) as feature to divide the multi-scale networks.

Specifically, the connectivity strength between DICCCOL landmarks is defined as follows:

$$C^n(\mathrm{L_i}, \mathrm{L_j}) = \mathrm{Fdensity} * \mathrm{averFA}$$

where $\mathrm{C^n}$ measures the connectivity strength between landmark L_i to L_j of subject n, and L_i is the ith landmark and $averFA$ is the averaged FA (fractional anisotropy) value along those fibers. Therefore, the bigger the number of fibers passing two landmarks is, the stronger the fibers' orientation consistency is, and thus the higher is the connectivity strength of the two landmarks. That is, $\mathrm{C}(\mathrm{L_i}, \mathrm{L_j})$ means how likely the landmarks L_i and L_j belong to one sub-network. As an example, Fig.1(b) illustrates

that those landmarks which have higher connectivity tend to be clustered into the same group. Here, it is assumed that the original spectral clustering algorithm [4] is adopted. For the convenience of visual evaluation, only two landmark groups are shown in Fig.1(b), that is, the red and green groups, respectively, which are likely to construct two sub-networks in the next section. This simple comparison experiment illustrates that the measurement can potentially reasonably group the DICCCOL landmarks. In order to keep the correspondences in other multiple scales, we averaged the connectivity strength between subjects, that is:

$$C = \sum_{n=1}^{N} C^n / N$$

Here, N is the number of subjects, and C^n is the connectivity matrix between the 358 DICCCOL landmarks of the nth subject. This averaged connectivity matrix aimed to eliminate inter-individual differences.

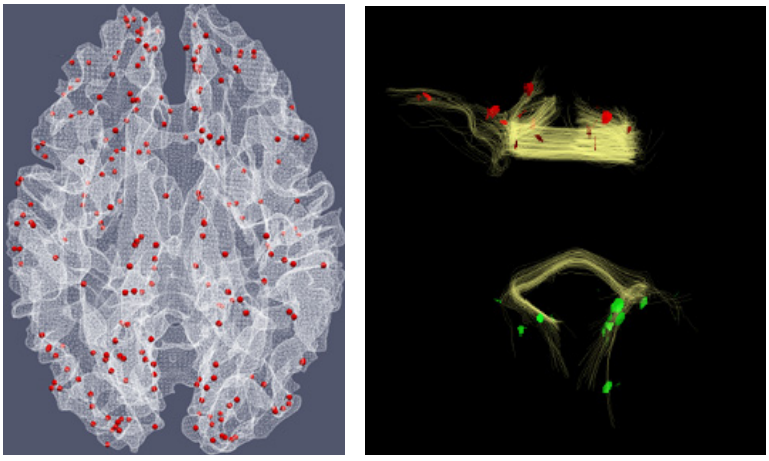

(a) (b)

Fig. 1. (a) An example of DICCCOL landmarks (red spheres). (b) Two sub-networks which have strong connectivity within each network. Spheres in two colors represent two clusters here.

2.4 Multi-scale Clustering

By taking each DICCCOL landmark as the node of an undirected weighted graph and connecting each pair of landmarks by an edge, the input of a spectral clustering algorithm is thus a Gaussian similarity matrix associated with the graph, which can be expressed as $W_{ij}(\delta) = \exp\left(-\frac{D(L_i,L_j)}{\delta^2}\right)$, where D is the landmark distance function, which measures the dissimilarity between landmark L_i to L_j. Naturally, D is defined as 1/C. Here, δ is the length scale of the Gaussian similarity function. The smaller it is, the smaller is the 'neighborhood' of a DICCCOL landmark.

Traditional spectral clustering methods need to specify different sets of parameters. As a consequence, the partition results may be subject to variations and uncertainty. In contrast, the multi-scale spectral clustering algorithm [2] can automatically explore the data structures (that is, learn the optimal δ) and infers different plausible values for the number of clusters from a random walk perspective. It tries to seek a reasonable partition of the graph such that the random walk stays within the same cluster and seldom jumps between different clusters. The algorithm offers the tree structure partition of data points, starting by separation in a large scale, and then recursively partitioning each of the resulting sub-trees. Fig.2 illustrates how the basic random walk spectral clustering determines the optimal number of clusters using the following functions:

$$\Delta(\mathrm{M},\delta) = \max_{\mathrm{k}} \left(\lambda_{\mathrm{k}}^{\mathrm{M}}(\delta) - \lambda_{\mathrm{k}+1}^{\mathrm{M}}(\delta)\right)$$
$$\mathrm{K}(\mathrm{M},\delta) = \arg\max_{\mathrm{k}} \left(\lambda_{\mathrm{k}}^{\mathrm{M}}(\delta) - \lambda_{\mathrm{k}+1}^{\mathrm{M}}(\delta)\right)$$

Here, λ_{k} is the *k*th eigenvalue, and $\lambda_{\mathrm{k}}^{\mathrm{M}}$ is λ_{k} to the *M*th power. The bigger $\Delta(\mathrm{M},\delta)$ is, the more distinguished is the structure revealed by it after a random walk of *M* steps. Here, δ for Fig.2 is fixed. However, we can learn δ and K simultaneously by changing δ. Thus each δ generates the curves of each Δ and K. For each δ, we identified the most distinguished structure with the highest Δ. Among all δ, we selected the most stable structure (staying the longest steps within the same cluster) with the highest stability measure. We recursively call the algorithm until the DICCCOL landmarks cannot be clustered furthermore, which finally resulted in a tree structure partition of data points. This procedure starts by separation in a large scale, and then recursively partitions each of the resulting sub-trees. More details of the algorithm can be found in [2, 13].

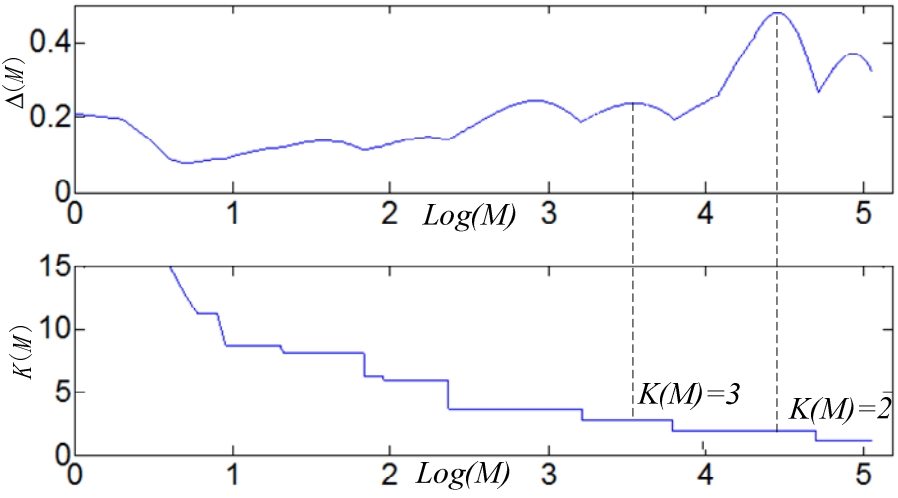

Fig. 2. The illustration for random walk spectral clustering

3 Experimental Results

3.1 Model of Multi-scale Brain Networks

The generated multi-scale brain networks via this proposed method are shown in Fig.3, each brain sub-network in one scale was divided again in the next scale, thus forming a tree structure from top-down. If we check from the left to the right, the most left column includes the clustered brain networks in each scale, and its sub-networks were shown in the right part. The clustered brain networks also include the leaf nodes from the upper layers. For the convenience of visual check, all the networks and sub-networks are represented as the overlay of all nine subjects at the same scale, and each brain sub-network was assigned with a different color. Altogether, the number of brain networks in scales 1~5 are 1, 5, 12, 17 and 20, respectively. We can see that the landmarks were reasonably clustered into groups across individuals.

Quantitatively, the consistencies within these sub-networks are stronger and stronger from scale 1 to 5. Figs. 4(a) and (b) show the connectivity strength matrices of every sub-network in scale 2 and 3, from which we can see that the consistency is higher for the higher scale. It is explained in (c), and the consistency curve also demonstrates this point. Here, the consistency is simply defined as the mean connectivity strength ("W" in section 2.4) within each network.

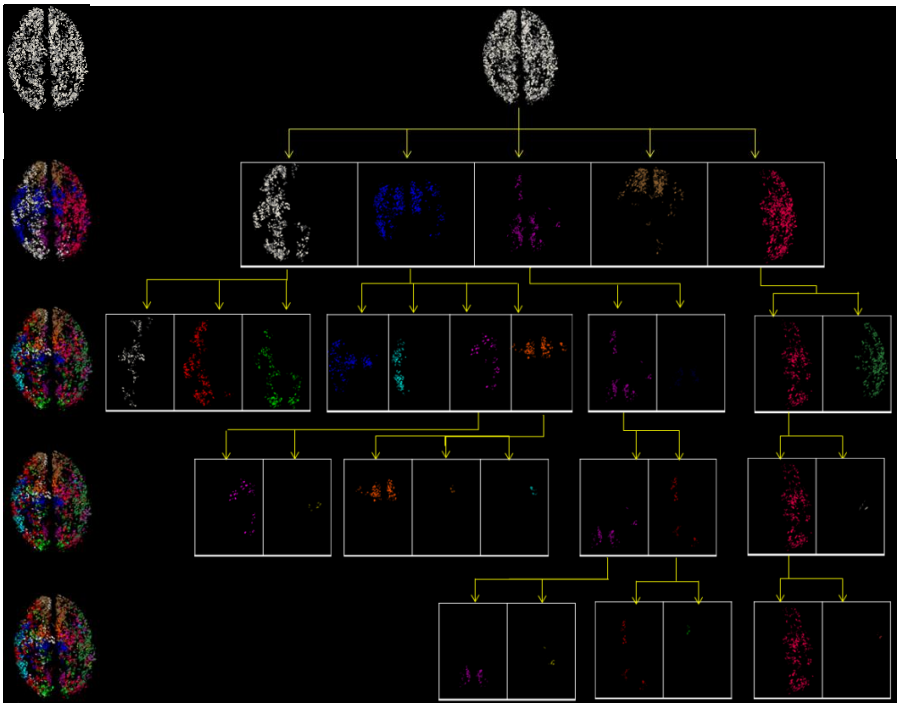

Fig. 3. Tree structure of the clustered multi-scale brain networks. Each sub-network in one scale was divided again in the next scale. All sub-networks are denoted by different colors, and each new sub-network in the next scale is designated a new color. The number of landmark clusters in scales 1~5 are 1, 5, 12, 17, 20 respectively.

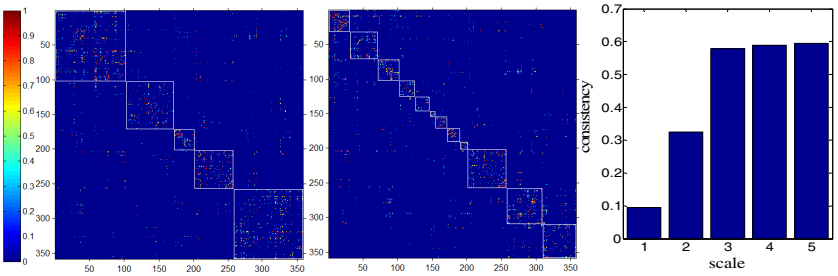

(a) Scale2 (b) Scale3 (c) Consistency curve

Fig. 4. (a) and (b): The connectivity strength matrices of every sub-network in scale 2 and 3. (c) The consistency curve at all scales.

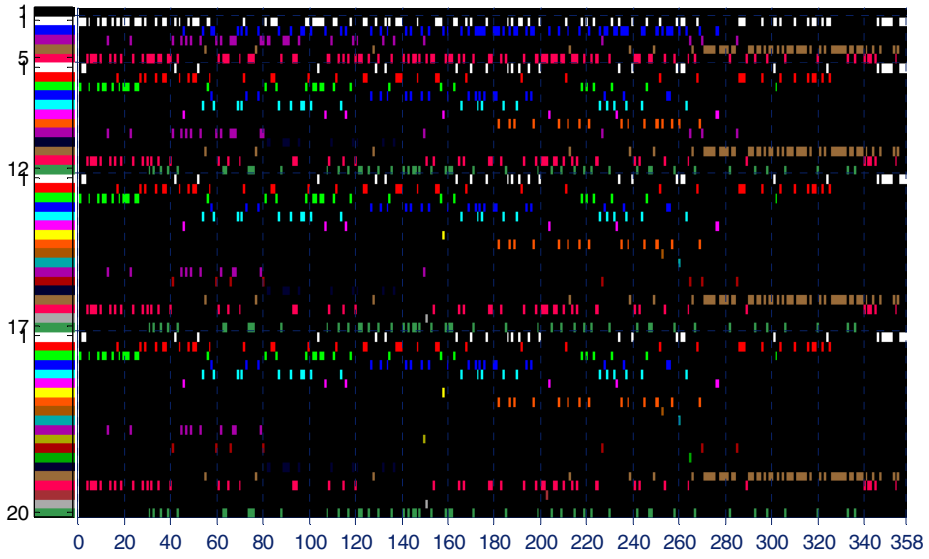

Fig. 5. The corresponding relationships between each sub-network and DICCCOL landmark ID included in each sub-network. The horizontal axis represents the 358 DICCCOL landmarks and the vertical axis represents every sub-network in scale 1~5. From top-down, the sub-network IDs are 1, 1~5, 1~12, 1~17 and 1~20 respectively. The color of each network and its corresponding landmarks are shown on the left and these colors are completely correspondent with those of all sub-networks in Fig.3. The colored rectangle in each row denotes the DICCCOL landmark ID included in this row sub-network.

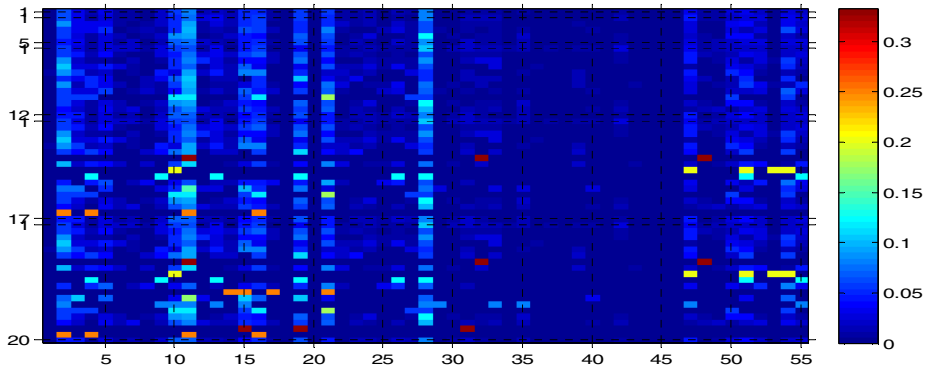

1.Action	2.execution	3.eexecution speech	4.imagination	5.inhibition
6.motor learning	7.observation	8.preparation	9.rest	10.Cognition
11.attention	12.language	13.orthography	14.phonology	15.semantics
16.language speech	17.syntax	18.memory	19.explicit	20.implicit
21.Memory working	22.music	23.reasoning	24. social cognition	25.soma
26.space	27.time	28.Emotion	29.anger	30.anxiety
31.disgust	32.fear	33.happiness	34.humor	35.sadness
36.Interoception	37.air hunger	38.baroregulation	39.bladder	40.hunger
41.osmoregulation	42.sexuality	43.sleep	44.thermoregulation	45.thirst
46.Perception	47.audition	48.gustationol	49.faction	50.somesthesis
51.pain	52.vision	53.color	54.motion	55.shape

Fig. 6. The percentage of functional roles of sub-networks. The horizontal axis represents the 55 functional behavioral domains used in the BrainMap database [7], which are listed in the bottom, and the vertical axis represents 55 sub-networks.

The significance of these sub-networks is that they can be cross-validated by the existing discovered functional or structural sub-networks [3]. Then, we provided a look-up table as shown in Fig.5, by which we can find how many sub-networks each network includes and which DICCCOL landmarks each sub-network includes. Furthermore, we can infer the functional roles of each sub-network by counting the functional roles of all landmarks within sub-network according to the recent meta-analysis results released in [3] based on the BrainMap database [7]. The percentage of each functional role of sub-network is shown in Fig.6. We can see that almost all the sub-network participate in some brain functional domains such as attention (11) and emotion (28), etc. We will provide a detailed functional analysis for sub-networks and fiber bundles in Section 3.3, because assigning fiber bundles with functional network roles is informative.

3.2 Prediction of Brain Networks in Individual Brains

We used another independent DTI dataset as a testing population to predict the multi-scale brain networks. The prediction procedure is straightforward under the guidance of the multi-scale network clustering results, since the Fig.5 already maps the multi-scale organization of the 358 DICCCOLs into the hierarchical brain networks. Because of the intrinsic correspondences established by the DICCCOLs,

the group-wise clustered network in the previous section can be readily used as the models to predict the tree structure for the new individual brains, once the DICCCOL landmarks are predicted in the new subjects. Fig.7 shows that the predicted brain networks from the nine different subjects. In each scale, there are three networks. For comparison, all nine brain networks which are same as those in Fig.3 are put in the first column, and the second column shows the nine predicted brain networks. The color of each sub-network is the same as that of sub-network in Fig.3. It is evident that the predicted networks are very similar to those model networks. These results demonstrate the robustness of the multi-scale network construction framework, as well as the reproducibility of the DICCCOLs and the associated brain networks.

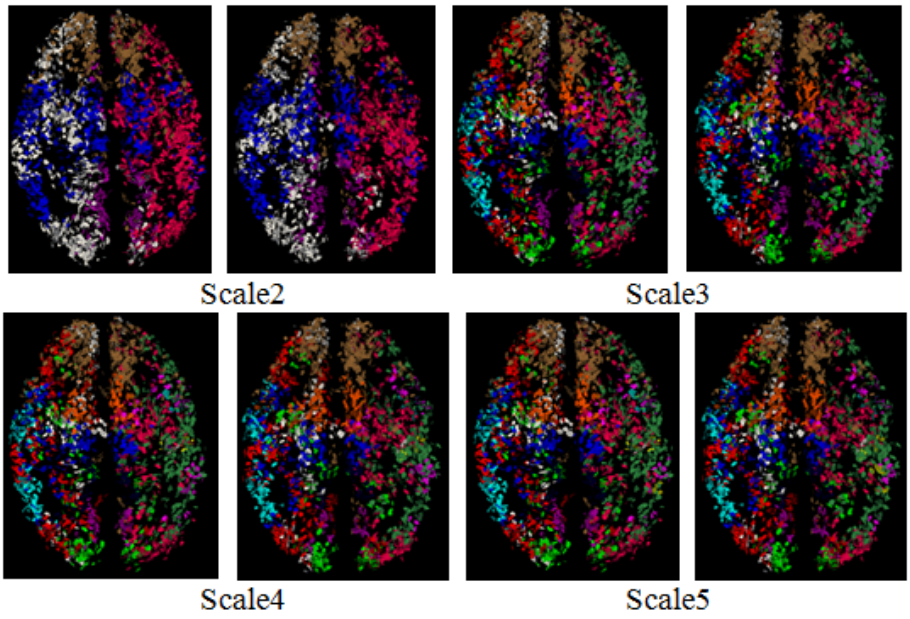

Fig. 7. The predicted multi-scale brain networks in nine different brains. Every brain network or sub-networks are overlaid by the nine different subjects. At each scale, for comparison, the left figure is the model network that corresponds to the left-most column in Fig.3, and the right is the predicted brain network.

3.3 Application in Identifying Common Fiber Bundles

Based on these multi-scale and corresponding brain networks obtained in section 3.1, we aim to identify common fiber bundles across individuals. First, we grouped all of the DTI-derived fibers connecting the pair of landmarks within each sub-network into the same fiber bundle, and then we selected those common fiber bundles across subjects at each scale. Fig.8 shows the common fiber bundles in scales 1-5. They have 1, 5, 11, 12 and 12 fiber bundles, respectively. The fiber bundles have the same colors as its corresponding sub-networks. It can be seen that there are stable and almost the

same fiber bundles in scale 3~5. It is evident that the multi-scale networks are able to effectively guide the identification of consistent fiber bundle.

Furthermore, we computed the averaged Hausdorff distances of corresponding fiber bundles in different subjects for scales 2~5, similar to that in [6]. Each fiber bundle was represented by its exemplar of Hausdorff distance when computing the Hausdorff distances of corresponding fiber bundles. Then the averaged Hausdorff distances denote the degree of correspondence and consistency among these fiber bundles from different subjects, as shown in Table 1. We can see that the averaged Hausdorff distance is relatively small in scales 2~5, indicating the accurate correspondence of fiber bundles. Finally, we averaged all the Hausdorff distances in the same scale, as shown in the last row, demonstrating that the fiber bundles and sub-networks are more consistent in higher scales. Table 1 also gives the corresponding relationships between fiber bundles and sub-networks, because not all sub-networks have its corresponding fiber bundles across different subjects.

Finally, Fig.9 shows that the identified fiber bundles in scale 2 and 3, in which we can see that the fiber bundles in scale 3 have more consistent shape. This demonstrated that sub-networks and corresponding fiber bundles are more consistent in higher scale. Also, guided by the relationships between fiber bundles and sub-networks, we assigned each fiber bundle with the corresponding the functional roles according to Fig.6, and the top 3 major functional roles are marked in Fig.9. It will be of interest for tract-based analysis [8, 9] in the future.

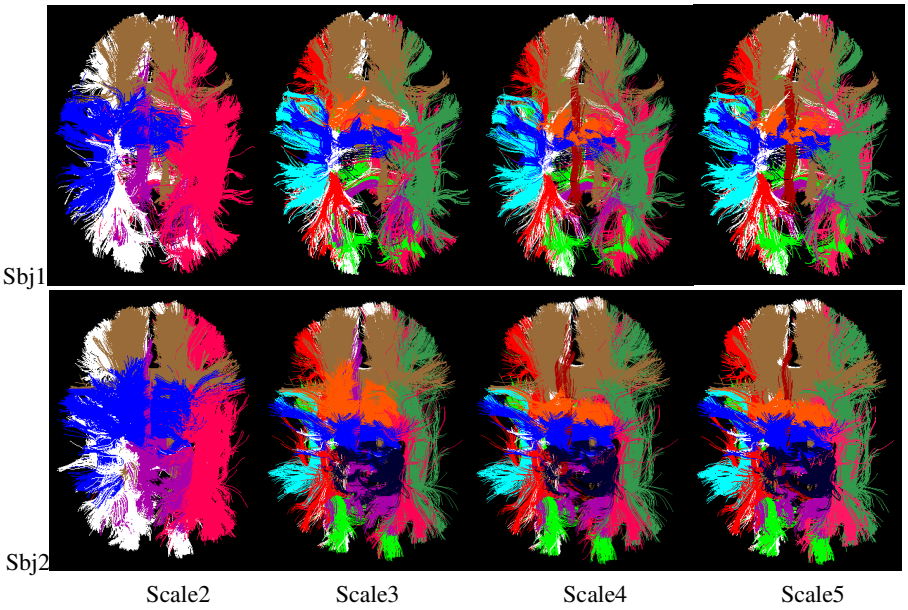

Fig. 8. The multi-scale common fiber bundles based on common brain networks from randomly selected two subjects. The fiber clusters were assigned with different colors, and the corresponding fiber bundles across different brains have the same color. Furthermore, these fiber bundles have the same colors as its corresponding sub-networks. The scales here correspond to the same set of scales in Fig. 3. The number of fiber bundles in scales 2~5 are 5, 11, 12, 12, respectively.

Table 1. The averaged Hausdorff distance (mm) of common fiber bundles between subjects in multi-scale and the corresponding relationships between fiber bundles and sub-networks. "null" represents that there are no common fiber bundles found in this sub-network.

	Scale2	Scale3	Scale4	Scale5
Sub-network ID	1: 13.84	1: 8.92	1: 8.92	1: 8.92
		2: 5.58	2: 5.58	2: 5.58
		3: 6.20	3: 6.20	3: 6.20
	2: 10.47	4: 6.49	4: 6.49	4: 6.49
		5: 4.02	5: 4.02	5: 4.02
		6: null	6: null	6: null
			7: null	7: null
		7: 3.81	8: 2.57	8: 2.57
			9: null	9: null
			10: null	10: null
	3: 8.49	8: 7.46	11: 2.87	11: 1.96
				12: null
			12: 3.58	13: 2.68
				14: null
		9: 2.95	13: 2.95	15: 2.95
	4: 9.56	10: 9.56	14: 9.56	16: 9.56
	5: 12.03	11: 8.73	15: 4.69	17: 3.59
				18: null
			16: null	19: null
		12: 6.94	17: 6.94	20: 6.94
average	10.88	6.42	5.36	5.12

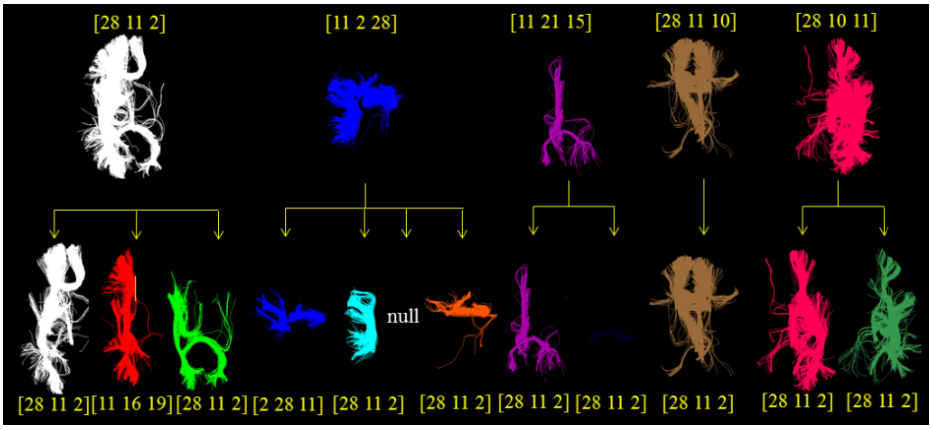

Fig. 9. The fiber bundles in scale 2 and 3. The first row shows the 5 fiber bundles identified via the 5 sub-networks at scale 2, and the second row shows the 11 fiber bundles identified via the 12 sub-networks at scale 3. The three major functional roles are marked by the indices of 55 networks in Fig.6 on each fiber bundle.

4 Conclusion

This paper proposed a novel method to construct the multi-scale common brain networks across individuals via an improved multi-scale spectral clustering of fiber connection strength. The obtained multi-scale common networks can be interpreted from the theory of functional integration of brain. The method has also been applied to identify common fiber bundles across subjects, and reasonable results were obtained. In general, our results on multi-scale brain networks and fiber bundles demonstrate the remarkable regularity of structural brain architecture, despite the noticeable variation across individuals as well. Experimental results have demonstrated that brain networks and fiber bundles are naturally organized in a multi-scale fashion, which can be reproduced and predicted across individuals and populations.

In the future, the work in this paper can be extended and enhanced in the following directions. First, the computational framework can be further extensively evaluated and validated by larger scale datasets. Second, these common multi-scale structural brain networks can be potentially widely used as the basis for many other brain network-level modeling and analyses such as functional interactions and dynamics. Also, the common multi-scale brain networks can be potentially used to examine the possible alterations in structural and functional connectivities in brain disorders. Finally, based on the multi-scale structural networks derived from DTI data, fMRI datasets can be used to model the multi-scale functional information flows on these structural networks for better understanding of the relationship between brain structure and function and for the elucidation of functioning mechanism of the brain.

References

1. Zhu, D., Li, K., Guo, L., et al.: DICCCOL: Dense Individualized and Common Connectivity-Based Cortical Landmarks. Cereb. Cortex 23(4), 786–800 (2012)
2. Azran, A., Ghahramani, Z.: Spectral methods for automatic multiscale data clustering. In: CVPR, pp. 190–197 (2006)
3. Yuan, Y., Jiang, X., Zhu, D., et al.: Meta-analysis of functional roles of DICCCOLs. Neuroinformatics (2012), http://www.ncbi.nlm.nih.gov/pubmed/23055045
4. von Luxburg, U.: A tutorial on spectral clustering. Statistics and Computing 17, 395–416 (2007)
5. Zalesky, A., Fornito, A., Harding, I.H., et al.: Whole-brain anatomical networks: does the choice of nodes matter? Neuroimage 50(3), 970–983 (2010)
6. Ge, B., et al.: Resting State fMRI-guided Fiber Clustering: Methods and Applications. Neuroinformatics (2012), http://www.ncbi.nlm.nih.gov/pubmed/23065648
7. Laird, A.R., Eickhoff, S.B., Kurth, F., Fox, P.M., Uecker, A.M., Turner, J.A., Robinson, J.L., Lancaster, J.L., Fox, P.T.: ALE meta-analysis workflows via the BrainMap database: Progress towards a probabilistic functional brain atlas. Frontiers in Neuroinformatics 3(23), 1–11 (2009)
8. Gerig, G., Gouttard, S., Corouge, I.: Analysis of Brain White Matter via Fiber Tract Modeling. In: IEEE EMBS, vol. 2, pp. 4421–4424 (2004)
9. Maddah, M., Grimson, W., Warfield, S.: Statistical Modeling and EM Clustering of White Matter Fiber Tracts. In: ISBI, vol. 1, pp. 53–56 (2006)

10. Zhang, D., Raichle, M.E.: Disease and the brain's dark energy. Nature Reviews Neurology 6(1), 15–28 (2010)
11. http://www.nitrc.org/projects/dicccol_0_1
12. Achard, S., Bullmore, E.: Efficiency and cost of economical brain functional networks. PLoS Comput. Biol. 3, e17 (2007)
13. Ge, B., Guo, L., Zhang, T., et al.: Construction of Multi-scale Brain Networks via DICCCOL Landmarks. In: ISBI (in press, 2013)
14. Kennedy, D.N.: Making Connections in the Connectome Era. Neuroinformatics 8(2), 61–62 (2010)
15. Hagmann, P., Cammoun, L., Gigandet, X., Gerhard, S., Grant, P.E., Wedeen, V., Meuli, R., Thiran, J.P., Honey, C.J., Sporns, O.: MR connectomics: Principles and challenges. Journal of Neuroscience Methods 194, 34–45 (2010)